Delay and Impairment in Brain Development and Function in Rat Offspring After Maternal Exposure to Methylmercury

Radonjic, Marijana; Cappaert, Natalie L. M.; de Vries, Erik; de Esch, Celine E. F.; Kuper, Frieke C.; van Waarde, Aren; Dierckx, Rudi; Wadman, Wytse J.; Wolterbeek, Andre P. M.; Stierum, Rob H.

Published in:
Toxicological Sciences

DOI:
10.1093/toxsci/kft024

Publication date:
2013

TOXICOLOGICAL SCIENCES
doi:10.1093/toxsci/kft024
Advance Access publication March 1, 2013

Delay and Impairment in Brain Development and Function in Rat Offspring After Maternal Exposure to Methylmercury

Marijana Radonjic,* Natalie L. M. Cappaert,† Erik F. J. de Vries,‡ Celine E. F. de Esch,*,[1] Frieke C. Kuper,* Aren van Waarde,‡ Rudi A. J. O. Dierckx,‡ Wytse J. Wadman,† André P. M. Wolterbeek,* Rob H. Stierum,* and Didima M. G. de Groot*,[2]

*TNO, 3700 AJ Zeist, The Netherlands; †Swammerdam Institute for Life Sciences, Center for NeuroScience, University of Amsterdam, 1090 GE Amsterdam, The Netherlands; and ‡Department of Nuclear Medicine and Molecular Imaging, University Medical Center Groningen, University of Groningen, 9700 RB Groningen, The Netherlands

[1]Present address: Erasmus MC, Department of Clinical Genetics, Rotterdam, The Netherlands.
[2]To whom correspondence should be addressed at TNO, PO Box 360, 3700 AJ Zeist, The Netherlands. Fax: +31(0)88 86 68 766.
E-mail: didima.degroot@tno.nl.

Received September 27, 2012; accepted February 9, 2013

Maternal exposure to the neurotoxin methylmercury (MeHg) has been shown to have adverse effects on neural development of the offspring in man. Little is known about the underlying mechanisms by which MeHg affects the developing brain. To explore the neurodevelopmental defects and the underlying mechanism associated with MeHg exposure, the cerebellum and cerebrum of Wistar rat pups were analyzed by [^{18}F]FDG PET functional imaging, field potential analysis, and microarray gene expression profiling. Female rat pups were exposed to MeHg via maternal diet during intrauterinal and lactational period (from gestational day 6 to postnatal day (PND)10), and their brain tissues were sampled for the analysis at weaning (PND18–21) and adulthood (PND61–70). The [^{18}F]FDG PET imaging and field potential analysis suggested a delay in brain activity and impaired neural function by MeHg. Genome-wide transcriptome analysis substantiated these findings by showing (1) a delay in the onset of gene expression related to neural development, and (2) alterations in pathways related to both structural and functional aspects of nervous system development. The latter included changes in gene expression of developmental regulators, developmental phase–associated genes, small GTPase signaling molecules, and representatives of all processes required for synaptic transmission. These findings were observed at dose levels at which only marginal changes in conventional developmental toxicity endpoints were detected. Therefore, the approaches applied in this study are promising in terms of yielding increased sensitivity compared with classical developmental toxicity tests.

Keywords: **neurodevelopment; methylmercury; [^{18}F]FDG PET functional imaging; field potential analysis; microarrays; neurotoxicity.**

The development of the brain is a highly complex and precisely timed process, which starts at gestation and continues throughout juvenile stages to adolescence. The early exposure of fetal and juvenile brain to environmental hazards may have deleterious effect on its development. Methylmercury (MeHg), which is found in some fish and shellfish, has harmful effects on the developing human nervous system. MeHg is the most stable organic form of mercury, and it has a high bioaccumulation potential (Clarkson and Magos, 2006; European Commission, 2006, 2010). The clinical findings in children exposed to MeHg poisonings in Japan (Harada, 1968; Takeuchi, 1985; Takizawa and Kitamura, 2001) and Iraq (Bakir *et al*., 1973) have revealed the extreme sensitivity of the developing brain to this compound and have triggered a series of animal studies aiming to determine the exact consequences of pre- and perinatal exposure to MeHg (Castoldi *et al.*, 2008). Neurobehavioral effects reported include altered motoric function and learning and memory disabilities; besides, *in vitro* studies showed inhibition of neuronal differentiation of neural stem cells (Johansson *et al.*, 2007). Nevertheless, the mechanism of action of MeHg is unknown, as are the differences in sensitivity of the various brain regions. Elucidation of these aspects would contribute to fine tuning of guidelines for developmental neurotoxicity testing and thus optimal protection of the offspring health.

The current guidelines for the assessment of MeHg developmental neurotoxicity focus on developmental landmarks and behavioral and extensive neuropathological/stereological surveys. The classical "No Observed Adverse Effect Level" (NOAEL) approach (Crump, 1984; Slob, 2002) aims to identify the highest dose level tested without an observed change in the (critical) endpoint. However, the fact that no change could be (statistically) observed at the NOAEL does not necessarily imply that there is no biologically relevant adverse effect present (European Food Safety Authority (EFSA), 2009). Previously, we have shown that by applying the advanced benchmark statistical approach, a significant dose-response effect of MeHg exposure can be identified in the conditions where classical NOAEL approach fails to detect these effects (Tonk *et al*., 2010).

In another related study with equivalent design, the relevance of MeHg effects was shown by neuron counting method, which detected statistically significant neuron loss at both juvenile and adult stage of MeHg-exposed rat pups. In the same study, the conventional neuropathological and behavioral guideline tests for developmental neurotoxicity (U.S. Environmental Protection Agency (U.S. EPA), 1996, 1998; Organisation for Economic Co-operation and Development (OECD), 2007) showed no statistically significant results (de Groot, personal communication). These observations demonstrate that conventional animal-based developmental neurotoxicity testing methods need to be complemented with more sensitive assays in order to accurately predict hazard and ultimately risk in man.

In this study, we investigate the early (lactation and weaning) and the late (adulthood) effects of pre- and perinatal MeHg exposure on structural and functional parameters of developing rat brain (cerebrum and cerebellum) by [^{18}F]FDG PET functional imaging, field potential analysis, and microarray gene expression profiling. Exposure equaled pre- and perinatal window proposed in U.S.-EPA Test Guideline for developmental neurotoxicity, i.e., from gestation day 6 (GD6) to postnatal day 10 (PND10) (U.S. Environmental Protection Agency, 1998). MeHg dose of 1.5 mg/kg was assessed in all assays and both tissues, and transcriptional profiling of cerebellum was also performed at lower MeHg doses (0.1, 0.4, and 1 mg/kg) to test the sensitivity of the method. We found a suggestive delay in onset of neural development and/or function and uncovered the molecular mechanisms underlying these defects. Importantly, we found that the early maternal dietary exposure to MeHg results in effects that persist to the adult stage of the exposed rats. In addition to the health relevance of these findings, our results show that methods for assessment of MeHg neurotoxicity used in this study provide an alternative method of superior sensitivity to classical toxicity testing protocols.

MATERIALS AND METHODS

Test substance. Methylmercury (MeHg), CAS 115-09-3, was obtained from Sigma-Aldrich, Zwijndrecht, The Netherlands.

Animals and animal husbandry. The *in-life* part of the study was carried out at the Animal Facilities of TNO Location Zeist, The Netherlands, as previously described (Tonk *et al*., 2010). Animal care and use were in accordance with Directive 86/609/RRC, which established the general principles governing the use of animals in experiments of the European Communities and with Dutch-specific legislation (The Experiments on Animals Act, 1977). Female and male Wistar rats (Crl-[WI]-WU BR), purchased from Charles-River Germany (Sulzfeld, Germany), were acclimatized for 12 days before mating at a ratio of 2 females:1 male. Animals were supplied with RM3 breeding diet (SDS, Witham, UK) and tap water, both *ad libitum*. Animals were housed in groups of four per sex in the animal facility with a 12-:12-h light:dark cycle and maintained at 22 ± 3°C and 30–70% humidity.

Study design and group selection. A regulatory developmental neurotoxicity study was carried out according to test guidelines US EPA OPPTS 870.6300/8600 (U.S. EPA, 1998). F0 female Wistar rats were orally dosed with MeHg dissolved in corn oil (Sigma). The MeHg was administered to the dams by gavage between GD6 and lactation day 10 (LD10) in the following concentrations: 0, 0.1, 0.4, 0.7, 1.0, 1.5, or 2.0 mg/kg body weight (BW) per day. The effects of MeHg on F1 offspring were studied during lactation, weaning, and adulthood by a series of conventional and more advanced tests.

The study started with 15 F0 female rats per group and an additional number of 8 females in the control group and also in the 1.5-mg MeHg groups. Per group, at least 10 dams with at least 10 pups each were selected for the neuro cohort. Litters were culled on PND8 to $n = 10$ pups/litter (5 male and 5 female pups). Two subsets (1 pup/sex/litter; 10 litters/dose group; all groups/subset) were selected for conventional behavioral testing and neuropathology as indicated in the test guideline. For PET imaging, five female F1 animals (four and a spare rat) from different litters (control group and 1.5-mg MeHg dose group) were selected and scanned at PND18, 22, 37, and 61. These time points were chosen—as near as possible—as proposed in the test guideline for conventional functional testing, i.e., 13, 17, 21, 61 ± 1 day (functional observational battery [FOB] and motor activity assessment [MAA]) but were limited by ethics—no PET scanning allowed below the age of PND17—and logistics—staggered start of experimentation and litters not born on the same day—leading to inclusion of PND37 to have another time point during adolescence. Likewise, animals for gene expression analysis and field potentials were selected as near as possible to weaning (PND21) and young adulthood (PND61 ± 1 day) as proposed for neuropathology survey in the test guideline (see below).

During lactation, developmental parameters (physical/sensory landmarks) were measured in both subsets of the neuro cohort, i.e., 2 male and 2 female pups/litter; 10 litters/group; all dose groups including control group. All behavioral tests like FOB and MAA (PND13, 17, 21, 61 ± 1 day), auditory startle response (PND23 ± 1 day), passive avoidance, and active avoidance tests (PND30 and 37 and PND60 and 67 (± 1 day), respectively) were carried out with 1 male and 1 female F1 animal/litter; 10 litters per group; all dose groups including the control group. Upto PND21, FOB and MAA were carried out in both subsets of the neuro cohort.

Subset 1 was sacrificed for neuropathology at PND21; subset 2 at PND70; the latter time point was needed to include active avoidance test for cognitive functioning (PND60 and 67 (± 1 day). Brains were dissected along neuroanatomical landmarks in such a way that left and right hemispheres could be used for different purposes (see below section "Brain samples preparation"). As such, still 10 animals/sex/group—all from different litters—were sampled for neuropathology (at PND21 and PND70); brain tissues (cerebrum and cerebellum separately) from at least five female F1 animals from different litters (control group and 1.5-mg MeHg group) were sampled for gene expression analysis ("genomics") during sacrifice (PND21 and PND70). Five female F1 animals from five different litters were selected for field potential measurements (control group and 1.5-mg MeHg dose group, at PND28 ± 3 days and at PND65 ± 3 days).

Here we report on the assessment of advanced testing technologies, i.e., *in vivo* [^{18}F]FDG PET imaging, *ex vivo/in vitro* field potential recording in brain slabs (hippocampus), and microarray gene expression/pathway analysis (cerebrum, cerebellum). For comparison of relative sensitivity, effects of conventional guideline testing is briefly touched upon (Supplementary material).

The study was accomplished in the spirit of Good Laboratory Practice.

BW and health. BW of the F1 animals was measured at different time points during experimentation: twice a week during lactation, starting on PND1 until PND21 (PND1, 4, 7, 10, 14, 17, and 21); weekly from PND21 onwards. Animals were checked daily for clinical signs of adverse effects. In the article, only the final outcome of effect of MeHg on BW is given in a brief summarizing table (Supplementary material).

Brain sample preparation. Brains were collected from the female F1 offspring immediately after sacrifice. Different brain parts were further dissected using neuroanatomical landmarks visible at the outer surface of the brain (de Groot *et al*., 2005a, b). Briefly, one coronal separation was made in between the cerebrum and olfactory bulb, and one separation was made in between the cerebellum and medulla oblongata/spinal cord at the dorsal end. Subsequently, the brain halves were separated along the midline. Then, the cerebrum was separated from the cerebellum by a coronal separation perpendicular to the midline. All brain parts were measured for size and weighed. Immediately thereafter, one brain half—alternating between the left and the right one (the first one was

chosen randomly)—was collected in formalin for neuropathology; the other was frozen for microarray analysis and toxicokinetic analysis of brain mercury levels. Left and right cerebellar and cerebral regions were also randomly assigned to either microarray analysis or toxicokinetic analysis. Frozen samples were stored at −80°C until further use. In this article, we only present the microarray analysis procedures and results (cerebrum and cerebellum separately).

Conventional neurodevelopmental toxicity testing. The effects on F1 offspring were studied assessing conventional guideline endpoints (BW, clinical signs, developmental landmarks, neuropathology, and behavior); cerebellar volume and neuron numbers were assessed with stereology as previously described (de Groot et al., 2005a, b). This part of the study is not included in this article and will be published elsewhere. However, for comparison of the sensitivity of the advanced technologies assessed and described here, the final outcome of the conventional tests is given in a brief summarizing table (Supplementary material).

[^{18}F]FDG PET imaging. Female rats exposed to 0 (control group, $n = 4$, and a spare animal) or 1.5 mg/kg MeHg daily (MeHg group, $n = 4$, and a spare animal) from GD6 until LD10 were subjected to repeated PET imaging. Brain glucose metabolism—a surrogate marker for brain activity—was assessed by static [^{18}F]FDG PET imaging on PND18, 22, 37, and 61. One animal in the MeHg group died between the third and fourth PET experiment. At the start of each PET experiment, the rat was injected ip with 21 ± 3 MBq [^{18}F]FDG. Immediately after the tracer injection, the animal was placed in an empty black wooden box (1 × 1 × 1 m) that was located in a dark room with monotonous background noise. This created circumstances with comparable external stimuli in conscious, active animals in which the tracer distribution could take place. Forty-five minutes after the administration of [^{18}F]FDG, the animal was taken from the box and anesthetized with 5% isoflurane gas in medical air (a mixture of 95% O_2 and 5% CO_2). The animal was positioned in a small-animal dedicated PET camera (Siemens/Concorde MicroPET Focus 220) with its brain in the center of the field of view. At the center of the field of view, the spatial resolution of the PET camera is 1.35 mm. Anesthesia was maintained with 2% isoflurane in medical air until the end of the PET procedure. A static emission scan was performed for 20 min, starting 50 min after tracer injection. Subsequently, a transmission scan was performed using an external ^{57}Co point source. The transmission scan lasted 515 s and was used for correction for attenuation and scatter of radiation by the tissue within the animal and the camera bed. After completion of the transmission scan, the animals were placed back into their cages to recover. Animals from the MeHg group and the control group were scanned in alternating order. PET data were iteratively reconstructed (OSEM 2D, four iterations) and corrected for decay, attenuation, scatter, and random coincidences. PET image analysis was performed using the Clinical Applications Packaging Program (CAPP5). The images were coregistered to an age-matched FDG template scan. Regions of interest (ROI) of cerebellum and hippocampus were drawn on the template FDG scan and transferred to the coregistered scan of the individual experimental animals. For each ROI, the radioactivity concentration was determined in Bq/cm^3 and normalized for injected tracer dose and BW to obtain a standardized uptake value (SUV), which is defined as:

$$\mathrm{SUV} = \frac{[\text{radioactivity concentration in tissue (Bq/g)} \times \text{body weight (g)}]}{\text{injected dose (Bq)}}$$

It is assumed that 1 cm^3 of brain tissue equals 1 g.

Statistical analysis of the differences in [^{18}F]FDG uptake in the individual brain regions between the MeHg group and the control group was performed with a two-sided, unpaired Student *t*-test. Differences between groups were considered statistically significant for $p < 0.05$.

Hippocampal slice preparation for extracellular field potentials. Rats of 28 (± 3) and 65 (± 3) days old (Fig. 1) exposed to 0 (control group) or 1.5 mg/kg MeHg were used for the analysis of the evoked local field potentials in hippocampal brain slices. Animals were decapitated, and the brains were quickly removed. The whole brain was placed for approximately 1 min into cold (0°C–4°C) artificial cerebral spinal fluid (ACSF containing 120mM NaCl, 3.5mM KCl, 1.3mM $MgSO_4$, 1.25mM NaH_2PO_4, 2.5mM $CaCl_2$, 10mM D-glucose, and 25mM $NaHCO_3$ saturated with carbogen: 95% O_2 and 5% CO_2 to set the pH at 7.4) before dissecting the brain tissue that contained the hippocampus. The tissue block was glued on a vibratome (Leica VT 1000S, Wetzlar, Germany), and horizontal slices of 400 µm thickness were prepared that contained the hippocampus. The slices were transferred into a holding chamber containing ACSF at room temperature. After a 30-min recovery period, the slices were transferred to a holding chamber onto a LCR membrane filter (MilliPore membrane filter, FHLC02500, PTFE hydrophilic membrane with 0.45 µm pore size; Millipore, Billerica, NA) placed on an ACSF-filled well, where they were kept at room temperature under a moistened carbogen atmosphere.

Extracellular recordings, electrical stimulation, and stimulation protocols. All recordings were performed at 31°C in a submerged slice chamber with ACSF as the perfusion medium. Extracellular field potential recordings were performed with borosilicate glass micropipettes (2–4 MΩ) filled with ACSF. The extracellular recording electrodes were placed in the CA1 stratum pyramidale (Fig. 3A1). Signals were amplified (1000×) with a custom-built amplifier and sampled at 5 kHz. Electrical stimulations were applied as a biphasic current pulse of 200 µs through a bipolar stimulation electrode (isolated stainless steel wires of 60 µm thickness with the tips 50–100 µm separated) that was placed over the Schaffer collaterals in stratum radiatum at the CA1–CA3 border (Fig. 3A1). The stimulation current for the threshold and the maximal response were determined for each slice individually, and the stimulus intensities were set using these two values as 0 and 100%, respectively. Two stimulation protocols were used to quantify the synaptic and network properties of the CA1 network. First, stimulus-response curves were constructed using double pulse stimulation protocols with interpulse intervals of 20 ms at current intensities of 0, 5, 10, 15, 20, 30, 40, 50, 80, and 100%. The second protocol used a fixed intensity (10 or 80%) and varying interpulse intervals from 20 to 500 ms. The minimum interval between any stimulation was 8 s.

Extracellular field potential analyses. All responses were means of three realizations, and the mean field potentials were analyzed using custom-made software (Matlab, The MathWorks Inc., Natick, MA). A local field potential recorded from the stratum pyramidale (Fig. 3A2) consists of the field equivalents of the synaptic potential (field excitatory postsynaptic potential—fEPSP) and a superimposed population spike (PS). The amplitude of the latter was calculated as schematically indicated in Figure 3A2. The ratio (R) PS2/PS1 was calculated to analyze the paired pulse interaction. One-way and three-way ANOVAs were used for statistical evaluation of the data (Matlab, The MathWorks, Inc.).

Genome-wide gene expression profiling. Rats of 21 and 70 days old exposed to 0 (control group), 0.1, 0.4, 1.0, and 1.5 mg/kg MeHg were selected for microarray analysis of cerebellum and rats exposed to 0 and 1.5 mg/kg MeHg for cerebrum. Prior to isolation of total RNA, cerebral and cerebellar brain regions were homogenized with a mortar and pestle under liquid nitrogen. Subsequently, the total RNAs derived from 3 to 6 biological replicate samples per treatment group (total 47 cerebellum and 21 cerebrum samples) were isolated using the NucleoSpin RNA II kit (Macherey-Nagel, Düren, Germany) RNA purification kit. RNA samples (eluted in water) were stored at −80°C before further processing. The isolated RNA samples were sent to ServiceXS BV (Leiden, The Netherlands) where they were processed according to Affymetrix protocols. In brief, RNA concentration was determined by absorbency at 260 nm with the Nanodrop ND-1000, and quality and integrity were verified using the RNA 6000 Nano assay on the Agilent 2100 Bioanalyzer (Agilent Technologies, Santa Clara, CA). Next, 2 µg of high-quality total RNA was used with the Affymetrix Eukaryotic One-Cycle Target Labeling and Control reagents to generate Biotin-labeled antisense cRNA. The quality of the cRNA was checked using the Agilent 2100 bioanalyzer. The labeled cRNA was further used for the hybridization to Affymetrix Rat230-2.0 Genome Genechips, harboring 31099 probe sets. After an automated process of washing and staining, absolute values of expression were calculated from the scanned array using the Affymetrix Command Console v1 software.

Microarray data preprocessing and quality control. Quality control microarray data were performed using simpleaffy and affyplm packages from the R/Bioconductor project through the Management and Analysis Database for MicroArray eXperiments (MADMAX) analysis pipeline, as previously described (Radonjic *et al*., 2009). Normalization of microarray data per tissue was performed through the same analysis pipeline using the library GC-RMA and employing the empirical Bayes approach for background correction followed by quantile normalization. The custom MBNI CDF-file (CustomCDF_rn230rnentrezg_v10.0.0), available at http://brainarray.mbni.med.umich.edu/Brainarray/Database/CustomCDF/CDF_download_v10.asp and http://nugo-r.bioinformatics.nl/NuGO_R.html was used to reannotate the probes to new probe sets, remove poor quality probes, and derive unique signal values for different probe sets representing the same gene. This resulted in gene expression values for 11,498 genes with unique identifiers. Data were additionally filtered based on expression signals. To pass filtering criteria, gene expression was required to have a value above 5 in at least one of the experiments, resulting in 10,422 genes in cerebellum and 10,229 genes in cerebrum.

Statistical analysis of microarray data, pathway analysis, and visualization. Differentially expressed genes were identified using the limma package, applying linear models and moderated *t*-statistics that implement empirical Bayes regularization of standard errors (Smyth, 2004). The statistical analyses were performed through the Remote Analysis Computation for gene Expression data (RACE) suite at http://race.unil.ch (Psarros *et al*., 2005). Doses of 0.1, 0.4, 1.0, and 1.5 mg/kg BW/day (GD6 to PND10) were tested on cerebellar gene expression. Gene expression under each MeHg dose treatment was compared with the control treatment (dose zero) per tissue and developmental stage (PND21 or PND70). To be statistically significant, fold change of gene expression was required to be either > 1.5 or < −1.5 and to have p value of < 0.01. The exception of the increasing dose effect (more differentially expressed genes with the increasing MeHg dose) at dose 1.5 mg/kg at PND70 may be due to the maternal cannibalism that we observed in this particular treatment group, indicating that this dose was too high for optimal viability. The surviving animals within this group showed large heterogeneity (resulting in relatively poor statistical power) of their gene expression response.

Hierarchical clustering and visualization of gene expression changes were performed in GeneSpring GX 7.3.1 software (Agilent Technologies). The expression value of each gene was normalized to the mean value of that gene across all conditions. The average expression per treatment group is plotted. The analysis of up- or downregulated Gene Ontology categories (GO, www.geneontology.org) in cerebrum was performed using Toxprofiler based upon the T-profiler algorithm (Boorsma *et al*., 2005). As input values, average $\log_2$ ratio values of gene expression levels (MeHg treatment vs. control group) of all 10,229 genes were used. T scores were considered significant if E value (Bonferroni corrected) was smaller than 0.05. This analysis results in T scores representing over-/underrepresentation of pathway-specific gene sets. Identification of overrepresented functional categories among differentially expressed genes in cerebellum was performed using DAVID Functional Annotation Clustering tool (Dennis *et al*., 2003). The analysis was performed using regulated Gene Ontology, Protein domains, Pathways, and Functional categories according to the default settings. Representative statistically significant GO functional categories and genes belonging to these categories are manually selected and reported in Figure 5B.

RESULTS

Female Wistar rat pups were exposed to MeHg via maternal diet during intrauterinal and lactational period from GD6 to PND10. The entire tested dose range was 0 (control treatment), 0.1, 0.4, 0.7, 1, 1.5, and 2 mg/kg of MeHg. During weaning and adulthood, cerebellum and cerebrum were sampled for the analysis by [^{18}F]FDG PET functional imaging, field potential analysis, and microarray gene expression profiling (Fig. 1). As a reference for sensitivity assessment of these alternative assays, conventional guideline tests for developmental neurotoxicity were also performed. In this article, a brief summary of the effects of MeHg found in the different conventional tests is given in Supplementary material. With exception of one parameter (i.e., sexual landmark "delayed vaginal opening"), none of the tests showed significant effect with NOAEL approach and a benchmark-advanced statistical method (Supplementary material).

Functional Imaging of Cerebellum and Hippocampus Suggests a Delay and Decrement in Brain Activity upon MeHg Exposure

As a surrogate biomarker for brain activity, glucose metabolism was assessed in a longitudinal manner by [^{18}F]FDG PET imaging at PND18, 22, 37, and 61. Cerebellum and hippocampus of the control group and the rats exposed to MeHg at dose 1.5 mg/kg were included in the analysis. Group comparison of [^{18}F]FDG uptake in cerebellum and hippocampus between MeHg-treated and control rats did not reveal significant differences at PND61. At PND18, however, [^{18}F]FDG uptake in cerebellum ($0.05 > p < 0.1$) and hippocampus ($0.05 > p < 0.1$) tended to be lower in MeHg-treated animals than in controls. On day 22, however, [^{18}F]FDG uptake in cerebellum ($p < 0.05$) and hippocampus ($0.05 > p < 0.1$) was (significantly) higher in MeHg-treated animals. On day 37, on the other hand, [^{18}F]FDG uptake was again significantly lower in the MeHg group than in controls both in cerebellum ($p < 0.05$) and hippocampus ($p < 0.05$). Strikingly, the pattern of [^{18}F]FDG uptake over time was markedly different between both experimental groups, whereas within each group, cerebellum and hippocampus showed similar uptake patterns (Fig. 2). As is illustrated in Figure 2, the FDG uptake apparently did not follow a gradual linear increase with age. In control animals, the average [^{18}F]FDG uptake in both hippocampus and cerebellum decreased between PND18 and 22 although not significantly. From PND22 to PND61, [^{18}F]FDG uptake in both brain regions increased, which resulted in [^{18}F]FDG uptake in both brain regions being significantly higher on PND61 than on either PND18 or PND22 ($p < 0.05$). In contrast, [^{18}F]FDG uptake in both hippocampus and cerebellum of MeHg-treated animals increased between day 18 and 22, then decreased between day 22 and 37, and increased again between day 37 and 61. None of these differences in tracer uptake between different days were statistically significant, except for the difference in [^{18}F]FDG uptake in hippocampus between PND18 and 22 ($p < 0.05$). At PND22 and PND37, the [^{18}F]FDG uptake levels of MeHg-exposed animals were similar to the ones of control animals at PND18 and PND22, respectively. These results might be suggestive for a possible delayed phase-shift pattern as depicted in Figure 2 by the artificial "15 days shift" graph, resulting from shifting the "dip" in [^{18}F]FDG uptake in the MeHg curve (PND37) toward the "dip" in the curve of the control group (PND22). It should be borne in mind, however, that [^{18}F]FDG uptake was measured only at four test ages. Brain activity in between the four measured time points is not known.

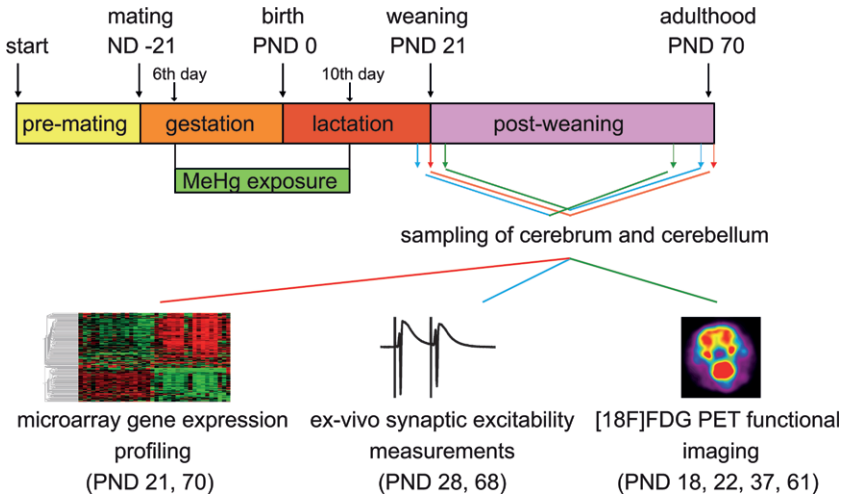

FIG. 1. Experimental design. Female Wistar rat pups were exposed to MeHg via maternal diet during intrauterine and lactation period (from GD 6 to PND10). During weaning and adulthood, cerebellum and cerebrum were studied and analyzed by [^{18}F]FDG PET functional imaging *in vivo, ex vivo/in vitro* field potential analysis, and *ex vivo* microarray gene expression profiling. This figure can be viewed in color online.

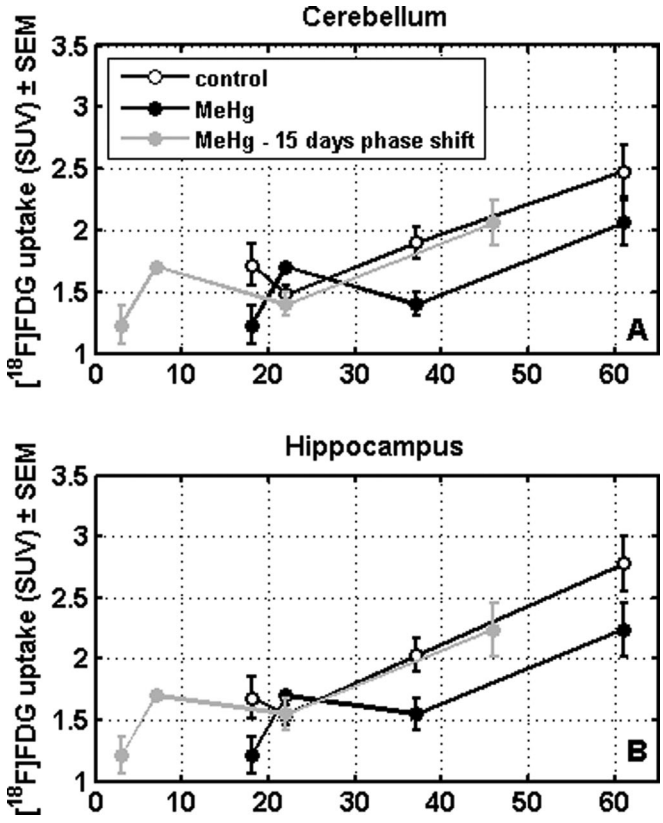

FIG. 2. Standardized [^{18}F]FDG brain uptake value (SUV) in cerebellum (A) and hippocampus (B) in rats exposed to 1.5 mg/kg of MeHg (black filled circles) and in control animals (open circles). Over time, [^{18}F]FDG brain uptake seemed to follow a typical pattern in both groups but different in time. High activity around day 18 in the control group can be explained by the fact that the animals are very active at this time point (comparable with high activity generally observed at this age in rats of this Wistar strain during MAA). Noticed that the [^{18}F]FDG uptake levels at the "dip" of the curves—PND37 in the MeHg group and PND22 in the control group—do not differ. The curve of [^{18}F]FDG uptake in MeHg animals was shifted 15 days—moving the "dip" at PND37 toward the "dip" at PND22 of the control group—suggesting delayed brain development in MeHg-treated animals (grey filled circles, dotted line).

MeHg Exposure Modifies Neurotransmission in the Hippocampus Assessed In Vitro Using Field Potentials

Basic neurotransmission was assessed in the pyramidal cell layer of the hippocampal CA1 region using field potential recordings in acute brain slices. The slices were obtained from control and MeHg-exposed rats (dose 1.5 mg/kg) at time points PND28 and PND68. In each group, a total of five rats were tested, coming from separate litters. From each rat, the field potentials were recorded in two brain slices, one from the left and one from the right hemisphere. The field potential amplitudes were defined per slice, and the data were averaged over hemispheres and rats. Stimulation of the afferent Schaffer collaterals (Fig. 3A1) induces a field potential in stratum pyramidale that consists of a representation of the synaptic currents (fEPSP) and a superimposed synchronized action potential (the PS, Fig. 3A2) evoked in the pyramidal neurons (Fig. 3A1). Stronger stimulation leads to a PS of larger amplitude; Figure 3B gives a typical result for the PND28. The threshold and the maximum stimulation intensity were set for each slice. The currents required to reach a threshold and to evoke a maximum field potential were not significantly different between the control and MeHg-exposed group at 28 and 68 days. The relation between PS amplitude and stimulus intensity is also observed in the MeHg-exposed group. Comparable stimulus response relations were obtained for the PND68 (data not shown). However, the maximum PS was significantly smaller at PND68 than at PND28 ($p < 0.01$).

Applying a second stimulus shortly after the first one reveals the short-term dynamics of the activated synapses. The PS2/PS1 ratio was determined for each stimulus pair given (Fig. 3A2). A ratio < 1 indicates paired pulse depression, and a ratio > 1 indicates paired pulse facilitation. Although the mean amplitudes of the PS1 and PS2 are not different (Fig. 3B), the short-term dynamics of the network do show effects of age and maternal MeHg exposure (Fig. 3C). The PND68 control group shows facilitation, primarily at the lower stimulus intensities, which was

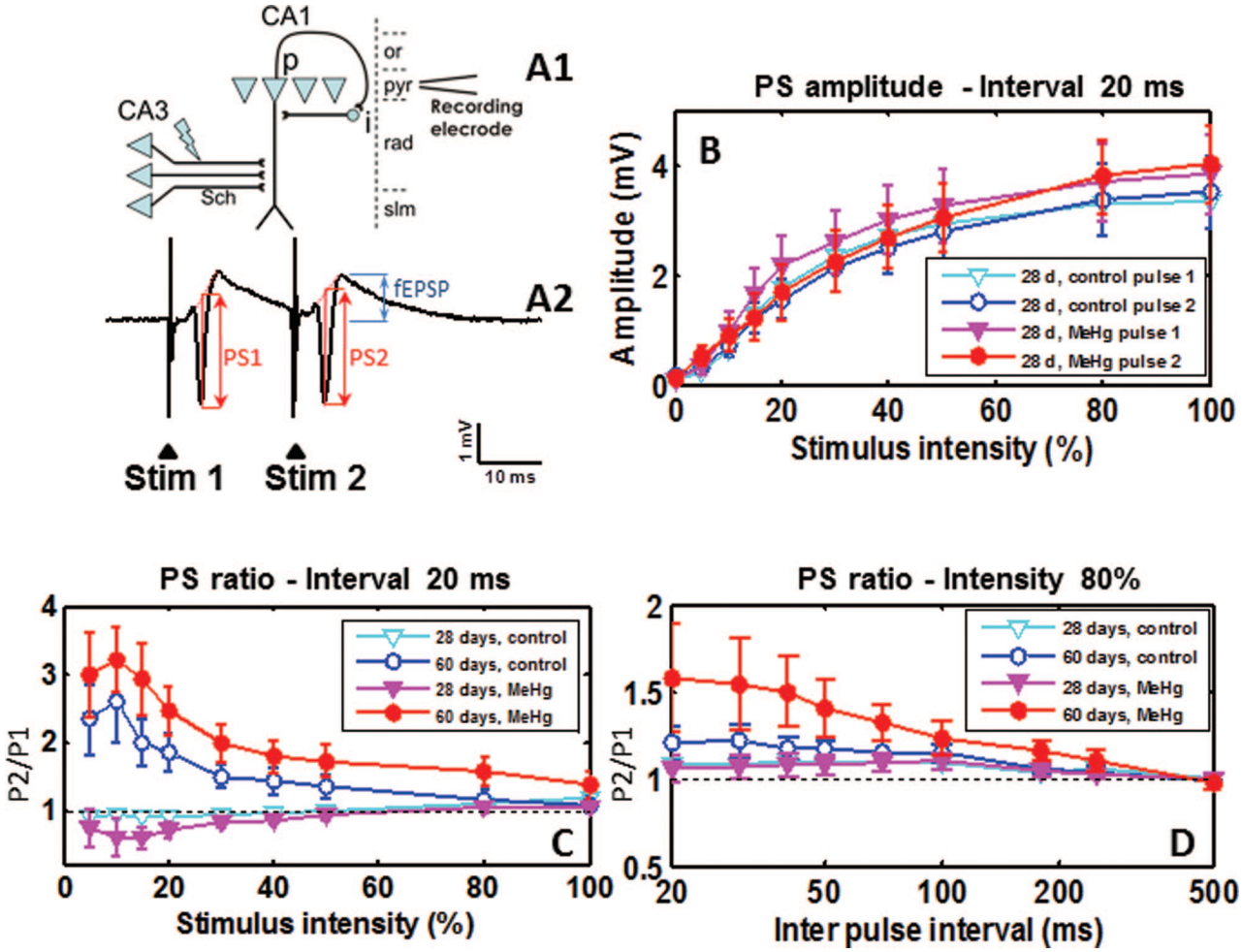

FIG. 3. (A1) A schematic drawing of the CA3 and CA1 region of the hippocampus of the rat. The triangles represent the cell bodies of the pyramidal cells (p), neatly aligned in the stratum pyramidale (pyr). The dendrites of the pyramidal cells are found in the stratum radiatum (rad) and the stratum lacunosum moleculare (slm). The Schaffer collaterals (Sch), axons of the CA3 pyramidal cells, project to the dendrites of the CA1 pyramidal cells. The axons of the CA1 pyramidal cells to inhibitory interneurons (i) within the CA1. These inhibitory interneurons project to the CA1 pyramidal cells in turn (feedback inhibition). The bipolar stimulation electrode was placed in parallel to the Schaffer collateral. The local field potentials were recorded in the stratum pyramidale. (A2) Local field potential recorded in the stratum pyramidale after double pulse stimulation of the Schaffer collaterals. The arrowheads (Stim1 and Stim2) indicate the moments of stimulation. The recording shows the extracellular representation of the field excitatory postsynaptic potential (fEPSP in blue; only indicated for Stim2) and the superimposed sharp negative deflection of the population spike (PS1 and PS2 in red); the determination of the PS amplitude is schematically explained. (B) Stimulus-response relations for the PS amplitude recorded in the stratum pyramidale of CA1 in response to Schaffer collaterals stimulation in hippocampal slices of PND28. Two stimuli, 20 ms apart, with the same stimulus intensity were applied; the intensity was stepwise increased from 0% (threshold for response) until 100% (saturation of response). Triangles represent the PS amplitude in response to the first stimulus (pulse 1); circles represent the PS amplitude in response to the second stimulus (pulse 2). The open symbols (in light and dark blue colors) represent the control group; the closed symbols (in pink and red colors) represent the MeHg-exposed group. The lines represent the mean data for each group ($n = 10$ [5 animals per group; left and right brain hemisphere/animal]); vertical bars represent SEM. (C) PS2/PS1 ratio as a function of stimulus intensity. The interpulse interval is 20 ms. Triangles represent PND 28, and circles represent PND 68. The open symbols (in light and darker blue) represent the control group, and the closed symbols (in pink and red) represent the MeHg-exposed group. The lines represent the mean data for each group ($n = 10$ [5 animals per group; left and right brain hemisphere/animal]); vertical bars represent SEM. (D) PS2/PS1 ratio as a function of stimulus interval for a fixed stimulus intensity of 80%. The markers and line colors are as in (C). The lines represent the mean data for each group ($n = 10$ [5 animals per group; left and right brain hemisphere/animal]); vertical bars represent SEM. This figure can be viewed in color online.

not observed in the PND28 control group (ANOVA, main effect of age: $F = 145.5$; $p < 0.01$; interaction age × stimulus intensity: $F = 5.62$; $p < 0.01$). In the MeHg-exposed group, at PND28, the PS2/PS1 ratio was changed into a small paired pulse depression, whereas at PND68, the group showed an enhanced paired pulse facilitation (ANOVA: main effect of MeHg exposure: $F = 4.43$; $p < 0.05$; interaction age × MeHg exposure: $F = 17.1$; $p < 0.01$).

The interval between the two stimuli is an important parameter that elucidates the underlying mechanisms. We systematically varied the interpulse interval between 20 and 500 ms and kept the stimulus intensity fixed at 80% to ensure action potential firing in response to the first pulse. In the control and the MeHg-exposed groups, only a very small facilitation was observed at PND28, which gradually vanished for

longer intervals and was not different between the two groups (Fig. 3C). At PND68, the facilitation in controls is larger than at PND28, and in the MeHg-exposed group, it is even larger (Fig. 3D) than in controls. A gradual decline of the facilitation was observed as a function of the time interval between P2 and P1 (Fig. 3D), (ANOVA main effect MeHg: $F = 5.13$; $p < 0.05$; main effect age: $F = 21.98$; $p < 0.01$; interaction MeHg × age: $F = 6.76$; $p < 0.01$). The same interpulse interval experiment was repeated at a stimulus intensity of 10%. In this case, there will be no action potential firing in response to the first pulse, and no feedback inhibitory interneurons will be recruited (Fig. 3A1). The facilitation of the fEPSP in the PND68 MeHg was higher compared with the facilitation in the PND68 control group (data not shown), similar to the 80% interpulse interval experiment.

Transcriptional Profiling Reveals a Phase Shift in Gene Expression of MeHg-Exposed Rats Compared with the Control Animals

To identify molecular mechanisms underlying effects of MeHg on rat brain development, cerebellar and cerebral RNA extracts at weaning (PND21) and adulthood (PND70) of the control and MeHg-exposed rat pups were subjected to microarray gene expression profiling using Affymetrix Rat 230-2.0 Chips. Cerebellar effects were investigated at MeHg dose range of 0 (control), 0.1, 0.4, 1, and 1.5 mg/kg. The investigated dose for cerebrum was limited to 0 and 1.5 mg/kg. In total, 10,422 and 10,229 genes were identified as expressed in cerebellum and cerebrum, respectively.

The analysis of differentially expressed genes (p value < 0.01 and absolute fold change > 1.5) reveals that MeHg affects larger number of genes at PND70 than at PND21 (Table 1). The annotated list of cerebellar and cerebral differentially expressed genes and their expression ratios compared with the control treatment is provided in Supplementary material. With the exception of the highest MeHg dose (1.5 mg/kg), the number of genes called significant in cerebellum increases with the exposure dose. To compare intensities of the gene expression changes across all conditions, differentially expressed genes in cerebellum and cerebrum were normalized to the mean value per gene and subjected to hierarchical clustering (Figs. 4A and B, respectively). This shows that in the control condition, there are many genes that are differentially expressed between the two developmental time points (PND21 and PND70). In animals exposed to MeHg at doses 1 and 1.5 mg/kg, cerebellar genes that are highly expressed at PND21 and lowly expressed at PND70 in the control condition are lowly expressed at PND21 and highly expressed at PND70 in MeHg-treated groups and vice versa. Such expression profiles of these genes thus appear phase shifted compared with the control groups. This suggested deregulation of appropriate timing of the neural gene expression program upon MeHg exposure resembles the suggestive MeHg-induced phase-shift pattern of the glucose uptake rate observed by [^{18}F]FDG PET imaging.

Molecular Mechanisms Underlying the MeHg Effects on Neurodevelopment

To identify molecular processes that are possibly affected by MeHg exposure in developing rat brains, differentially expressed genes in cerebrum and cerebellum were subjected to pathway analyses. The results reveal that many of MeHg affected genes are involved in nervous system development, including both structural and functional aspects (Figs. 5A and B). In cerebrum, all GO categories related to neurodevelopmental processes are downregulated (Fig. 5A). Specifically, pathways related to structural aspects of brain development (e.g., nervous system development, ensheathment of neurons, myelination, cytoskeleton organization, and biogenesis) are significantly repressed at PND21, whereas PND70 is predominantly characterized by significant repression of pathways related to synaptic transmission and brain function (synaptic vesicle, transmission of nerve impulse, behavior). The analysis of overrepresented GO categories in cerebellum revealed that also in this brain part, MeHg significantly affects processes related to neural function and development, such as synaptic transmission, neuron projection, transmission of nerve impulse, dorsal/ventral pattern formation, and nervous system development (Fig. 5B).

Detailed examination of genes affected by MeHg cerebellum reveals expression changes in many developmental regulators (*Foxg1, Ctxn* [*cortexin*], *Gda, Ptms, Akt, Basp, Lhx2, Arsb*), developmental phase–associated genes (*Cxxc4, St18, Atrx, Bmpr1c, Fut9, Kif1b, Mtap2, and PPARgC1b*) and genes involved in small GTPase signaling pathways regulating cell growth and proliferation (Supplementary material). Apart from the structural aspects, representatives of all processes required for synaptic transmission are identified as significantly affected by MeHg. This includes neurotransmitters (*Cck* [cholecystokinin], *Pmch, Pcsk1n*), neurotransmitter synthesis gene (*Gad2*), neurotransmitter receptors (*Cnr1* [cannabinoid receptor 1], *Gabrb3* [$GABA_A$ receptor], and *LOC289606* [$GABA_A$ receptor homolog]), synaptic vesicle docking/transport/neurotransmitter secretion genes (*Spt5, Syn1a*, *Cplx2*, *Myo5a, Slc6a6, Lin7c, Lin7a, Exoc8*), voltage-gated Ca^{2+} channels (*Cacnb4, Ryr3, LOC689560*), Ca^{2+}/calmodulin binding proteins and kinases (*Camkk2, Camk2n1, Camk4, Marcksl1*), and regulators of synaptic plasticity (*Nrgn* [neurogranin], *Ddn* [dendrin], and *Rnf39*). Particularly marked repression of several genes regulating brain development (*Foxg1, Gda*) and

TABLE 1
Number of Significantly Differentially Expressed Genes Upon MeHg Exposure at PND 21 and 70

	Cerebellum				Cerebrum
MeHg (mg/kg)	0.1	0.4	1	1.5	1.5
PND21	6	7	8	18	11
PND70	22	23	115	34	14

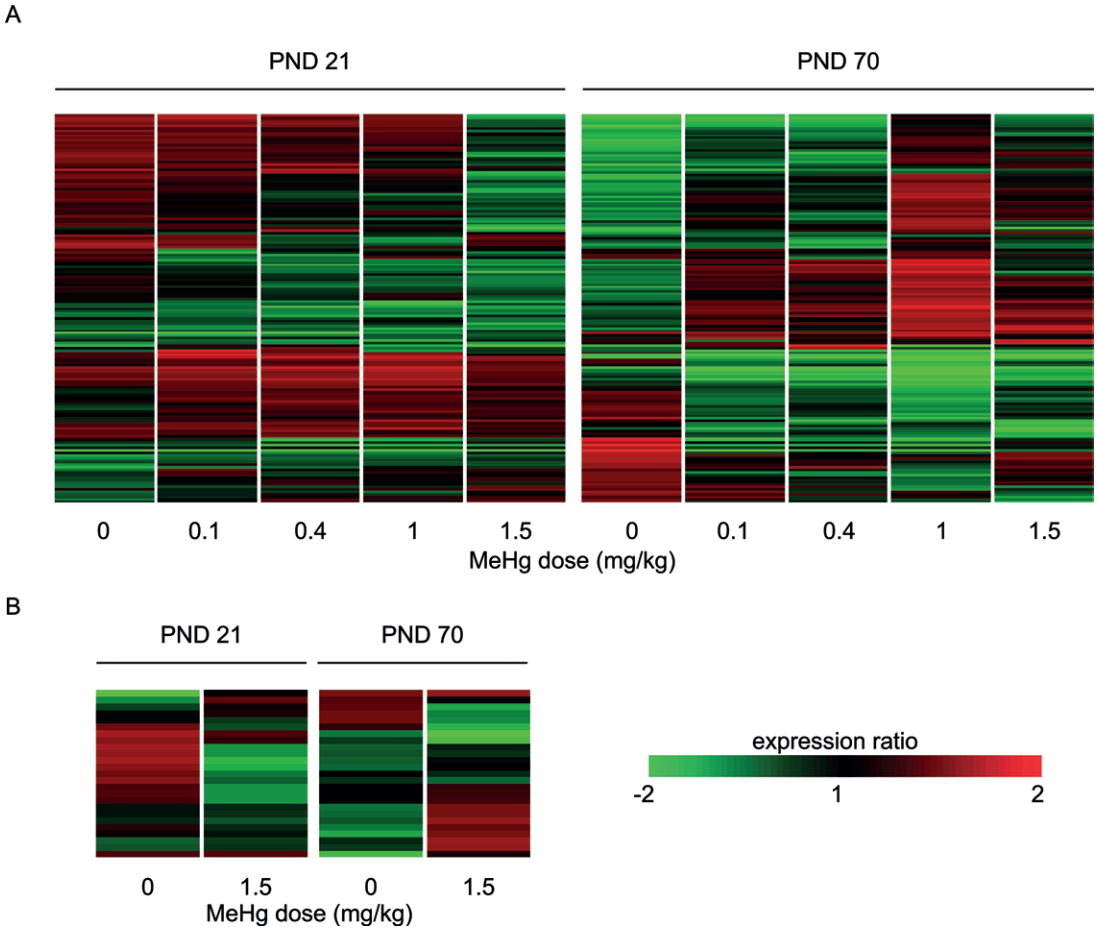

FIG. 4. (A) A heat map showing expression of genes differentially expressed in cerebellum under at least one of the time points and doses of MeHg compared with the control condition (0 mg/kg) ($n = 159$). The expression value of each gene was normalized to the mean value of that gene across all conditions. The average expression per treatment group is plotted. (B) Similar to (A) for genes differentially expressed in cerebrum under MeHg dose 1.5 mg/kg compared with the control condition (dose 0 mg/kg) ($n = 25$). This figure can be viewed in color online.

function (*Cck* and *Nrgr*, long-term potentiation and learning regulator) is observed at PND70, showing that pre-/perinatal MeHg exposure has distinct long-term effects on brain structure and function. In addition to effects on neural structure and function, a number of differentially expressed genes point to effects of MeHg on the brain immune system (*Nrgn, Akt1, Adam10, Myo5a*).

Together, microarray gene expression profiling corroborates findings regarding delay and decrement in brain function and compromised functionality of neurotransmission discovered by [^{18}F]FDG PET imaging and field potential analysis and identifies key regulators of these processes.

DISCUSSION

In the study presented here, maternal exposure to MeHg was studied in rat offspring using [^{18}F]FDG PET functional imaging, field potential analysis, and microarray gene expression profiling. For PET and field potential analyses, a dosage of 1.5 mg MeHg/kg BW/day (GD6-LD10) was used; for gene expression profiling, low dosages of 0.1, 0.4, and 1.0 mg MeHg/kg were studied in addition.

MeHg is a well established neurotoxin both in humans and animals. The developing brain appears more vulnerable to the toxic effects of MeHg than the adult, and much lower dosages are required to generate deleterious effects (Costa *et al.*, 2004; Franco *et al.*, 2006; Grandjean and Landrigan, 2006; Kjellstrom *et al.*, 1989; Manfroi *et al.*, 2004). Humans are exposed to MeHg, for example, through the consumption of fish and shellfish. After absorption through the digestive tract, MeHg can penetrate the blood-brain barrier and the placenta (Choi, 1989; Clarkson and Magos, 2006). Because of its long half life in the human body, it accumulates in the brain where it causes damage to the central nervous system (Coccini, 2000; Spyker, 1972). MeHg has been studied extensively, and adverse effects on brain development and animal behavior (functional) have been found (Weiss, 2005). Structural damage to the developing brain is diffuse, whereas damage is restricted

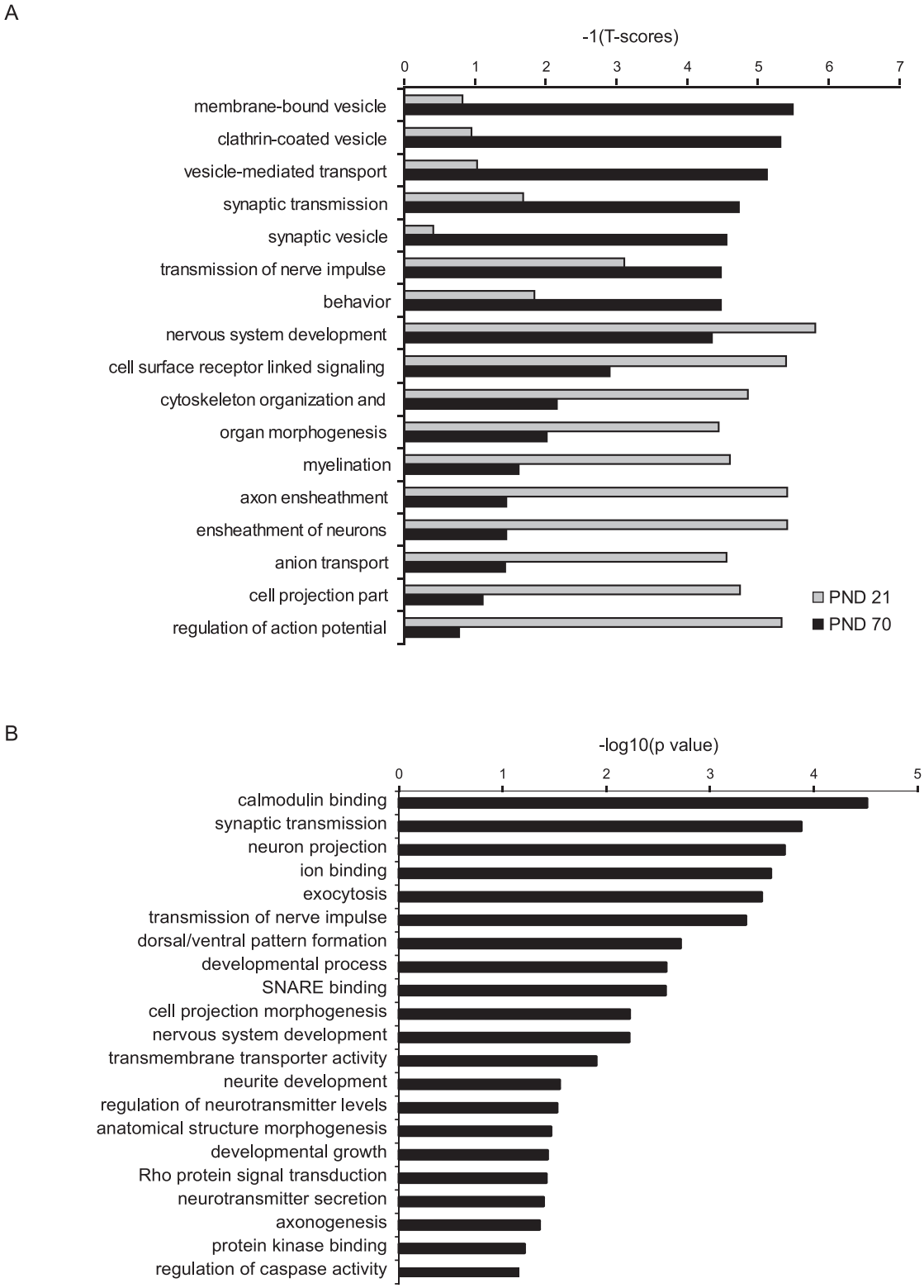

FIG. 5. (A) The selected GO functional categories significantly downregulated (negative *T* values) in cerebrums of MeHg-exposed rats at PND21 and PND70. Pathways related to brain structure are mostly affected at PND21, whereas pathways related to brain function are affected at PND70. The Bonferroni corrected *E* value < 0.05 is at |T| > 4. (B) The selected GO functional categories significantly overrepresented among 159 genes differentially expressed in cerebellum under at least one of the doses of MeHg compared with the control condition.

to cerebellum and visual cortex in the adult brain (Burbacher *et al*., 1990). Prenatal exposure is related to abnormal neuronal migration and deranged cerebral cortical organization. Children exposed to MeHg may be mentally retarded and show decreased IQ, impaired movements, visuospatial perception, and speech (Castoldi *et al*., 2008; Harada, 1995; Grandjean *et al*., 1997; Kjellstrom *et al*., 1989). Effects on animal behavior include, among others, reduced motor activity (Björklund, 2007), a decrease in memory ability (Carratù *et al*., 2006; Daré *et al*., 2003; Sakamoto, 2002) and learning (Paletz *et al*., 2006). Mechanisms underlying mercury-induced neurotoxicity have been focused on for many years. To mention, disruption of calcium homeostasis or induction of oxidative stress via overproduction of reactive oxygen species or reduction of antioxidative defenses is likely to be critical factors in MeHg-induced cell damage, as are interactions with sulfhydryl groups (Ceccatelli *et al*., 2010; Farina *et al*., 2011a, b; Giordano and Costa, 2012). Yet, the molecular mechanisms mediating MeHg-induced neurotoxicity are not completely understood.

In this study, we investigated mechanisms underlying neurodevelopmental defects associated with maternal exposure to MeHg. [^{18}F]FDG PET functional imaging of cerebellum and hippocampus, the analysis of functional neurotransmission in the hippocampus, and microarray gene expression profiling of cerebrum and cerebellum were employed to assess the effects of MeHg exposure on structure and function of rat brains in juvenile and adult stages of development. The rat has been reported to be a good model to study developmental neurotoxicity of MeHg (Costa *et al*., 2011; Giordano and Costa, 2012).

We find that MeHg causes structural defects and delay and decrement in (onset of) neural activity in both cerebrum and cerebellum of Wistar rat pups. Importantly, although the pups were exposed to MeHg early in developmental stage (from GD6 to PND10, i.e., lactation) and the mercury levels in the brain already returned to control level on PND21 (data not shown), the significant effect on neural structure and function persisted into adulthood (PND70) on a functional and molecular level.

The development of the brain is a highly complex process in which timing of events is crucial to ensure that development proceeds normally (Mai and Ashwell, 2004). One of the main observations in this study is that this timing is disrupted in animals exposed to MeHg in both cerebrum and cerebellum. This is evident from the gene expression profiling, which shows that the specific timing of transcriptional programs associated with early and late developmental stage is disturbed in MeHg-treated groups. Genes that are required to be highly expressed at early stage and lowly expressed at the late stage in the control condition show an opposite pattern of expression in MeHg-treated groups. Indeed, many of such genes with phase shift in timing of expression are described as developmental phase–associated genes. [^{18}F]FDG PET imaging data appear to be in agreement with gene expression findings, as PET imaging results also seem to concur with a delayed glucose consumption pattern in hippocampus and cerebellum of MeHg-exposed animals. The peak in [^{18}F]FDG uptake observed in the control group around day 18 can be explained by the fact that rats of this Wistar strain are very active at this time point as is generally seen during MAA where activity at PND17 is larger than that measured at PND21. In the hippocampus of the MeHg group, [^{18}F]FDG uptake significantly increased between PND18 and PND22. The fact that this peak in brain activity—[^{18}F]FDG uptake—is found at a later time point in the MeHg group (PND22) where the activity in the control group is already going down (as in MAA) supports the suggestive neurodevelopmental delay depicted in the "15 days shift" in Figure 2. Clearly, a neurodevelopmental delay of 15 days early in life does not seem realistic. Most likely, MeHg interfered with neurodevelopmental processes at a critical time window of brain development inducing a small delay, which may even go unrecognized. Yet, neurodevelopment may increasingly lag behind with age, becoming apparent later in life during adulthood or senescence (Grandjean and Herz, 2011). Together, these results and gene expression findings suggest that MeHg induces a delay in onset of brain development and function both in cerebellum and cerebrum.

The assessment of MeHg effects at two time points allows us to discriminate between early (weaning) and late (adulthood) neurodevelopmental defects caused by pre-/perinatal exposure to MeHg. Surprisingly, the effect of MeHg is amplified and persisting at the adult stage, despite the fact that MeHg has been eliminated from the system long time ago. This is manifested by a higher number of differentially expressed genes at PND70 compared with PND21, persisting lower glucose uptake rate (also) at PND61 and increase in potentiation of hippocampal neurons specifically at PND68. In the cerebrum, phase-specific MeHg effects are evident from pathway analyses of differentially expressed genes. Pathways related to structural aspects of brain development are significantly repressed at PND21, whereas PND70 is predominantly characterized by significant repression of pathways related to synaptic transmission. This suggests that pre- and perinatal MeHg exposure at first instance causes impaired development of morphological features of the brain, which is in line with a previous report on significant neuron loss at PND21 (de Groot, personal communication), whereas at the adult stage, MeHg-caused impairment in cerebrum is mostly apparent in brain function disorders.

Functional changes at the adult stage by MeHg are also shown by the analysis of neurotransmission in hippocampus. The extracellular field potential recordings in the hippocampus provide a marker for synaptic transmission, and double pulse stimulation can elucidate some characteristics of the underlying mechanisms. MeHg exposure causes increased paired pulse facilitation at PND68, which is generally explained by an increase in neurotransmitter vesicle release. This increase could have several underlying causes, but one of the most common explanations at lower stimulus intensities (Fig. 3C) and one that is expected to gradually decline with stimulus interval

(Fig. 3D) is the residual calcium hypothesis (Katz and Miledi, 1968; Miledi and Thies, 1971; Parnas *et al*., 1982; Zucker, 1989). Additionally, network properties could also contribute to the change in vesicle release because activation of pyramidal cells leads to activation of feedback inhibition of the GABAergic interneurons (Fig. 3A1), which could in turn inhibit the second PS in the double pulse protocol (Stanford *et al*., 1995). However, at PND68, there is a strong paired pulse enhancement with an interval dependency that strongly suggests that the residual calcium is underlying it.

One of the most prominently differentially expressed genes under MeHg treatment is Neurogranin (*Nrgn*), regulator of synaptic plasticity (Díez-Guerra, 2010; Prichard *et al*., 1999). *Nrgn* is significantly repressed in cerebellum at both PND21 and PND70, even at doses as low as 0.4 and 0.1 mg/kg MeHg, suggesting that this factor may be responsible for regulating MeHg-induced functional impairment. Another severely repressed gene in cerebellum is *Foxg1* (−8.3-fold downregulation at dose 1 mg/kg at PND70). FOXG1, also known as Brain factor 1, has been found to play an important role in the establishment of the regional subdivision of the developing brain and in the development of the telencephalon (Tao and Lai, 1992). In addition, *Foxg1* mutations are associated with the neurodevelopmental disease Rett syndrome. Considering its severe repression upon MeHg exposure, it is plausible that this factor may be important for regulating MeHg-mediated structural defects.

Finally, in our study, the effects of MeHg observed by [^{18}F]FDG microPET functional imaging, functional neurotransmission analysis, and microarray gene expression profiling were not identified by classical methods included in current guidelines for neurotoxicity testing. Such improved sensitivity of detection of relevant neurotoxic effects implies that the current testing protocols for neurotoxicity could be enhanced by employment of innovative methods in addition (or as an alternative) to conventional guideline endpoints. This may have important implications on juvenile health care but also on improvement of procedures for animal testing, such as increased efficiency and sensitivity and decrease of number of animals used, time, and costs of testing.

SUPPLEMENTARY DATA

Supplementary data are available online at http://toxsci.oxfordjournals.org/.

ACKNOWLEDGMENTS

The authors like to thank the teams of Mr Gerard Beek (Animal Facilities/Biotechnique) and Mrs Lidy van Oostrum (Histotechnique) for taking care of the animals and the processing of tissues. Especially, the excellent skills of Mrs Linda vd Horst and Marlies Otto during the in-life phase of the study (including also their assistance during field potential measurements (at UvA, Amsterdam) are acknowledged. The inspiring discussions with the enthusiastic students Anke Wesselius, Bart Voet, Rianne Nederlof, and Mark Bogaart on the relevance of [^{18}F]FDG PET imaging for developmental neurotoxicity testing and contribution to Animal 3Rs (Replacement, Refinement, Reduction) are much appreciated.

REFERENCES

Bakir, F., Damluji, S. F., Amin-Zaki, L., Murtadha, M., Khalidi, A., al-Rawi, N. Y., Tikriti, S., Dahahir, H. I., Clarkson, T. W., Smith, J. C., *et al.* (1973). Methylmercury poisoning in Iraq. *Science* **181,** 230–241.

Björklund, O., Kahlström, J., Salmi, P., Ogren, S. O., Vahter, M., Chen, J. F., Fredholm, B. B., and Daré, E. (2007). The effects of methylmercury on motor activity are sex- and age-dependent, and modulated by genetic deletion of adenosine receptors and caffeine administration. *Toxicology* **241,** 119–133.

Boorsma, A., Foat, B. C., Vis, D., Klis, F., and Bussemaker, H. J. (2005). T-profiler: Scoring the activity of predefined groups of genes using gene expression data. *Nucleic Acids Res*. **33**(Web Server issue), W592–W595.

Burbacher, T. M., Rodier, P. M., and Weiss, B. (1990). Methylmercury developmental neurotoxicity: A comparison of effects in humans and animals. *Neurotoxicol. Teratol*. **12,** 191–202.

Carratù, M. R., Borracci, P., Coluccia, A., Giustino, A., Renna, G., Tomasini, M. C., Raisi, E., Antonelli, T., Cuomo, V., Mazzoni, E., *et al.* (2006). Acute exposure to methylmercury at two developmental windows: Focus on neurobehavioral and neurochemical effects in rat offspring. *Neuroscience* **141,** 1619–1629.

Castoldi, A. F., Johansson, C., Onishchenko, N., Coccini, T., Roda, E., Vahter, M., Ceccatelli, S., and Manzo, L. (2008). Human developmental neurotoxicity of methylmercury: Impact of variables and risk modifiers. *Regul. Toxicol. Pharmacol*. **51,** 201–214.

Castoldi, A. F., Onishchenko, N., Johansson, C., Coccini, T., Roda, E., Vahter, M., Ceccatelli, S., and Manzo, L. (2008). Neurodevelopmental toxicity of methylmercury: Laboratory animal data and their contribution to human risk assessment. *Regul. Toxicol. Pharmacol*. **51,** 215–229.

Ceccatelli, S., Daré, E., and Moors, M. (2010). Methylmercury-induced neurotoxicity and apoptosis. *Chem. Biol. Interact*. **188,** 301–308.

Choi, B. H. (1989). The effects of methylmercury on the developing brain. *Prog. Neurobiol*. **32,** 447–470.

Clarkson, T. W., and Magos, L. (2006). The toxicology of mercury and its chemical compounds. *Crit. Rev. Toxicol*. **36,** 609–662.

Coccini, T., Randine, G., Candura, S. M., Nappi, R. E., Prockop, L. D., and Manzo, L. (2000). Low-level exposure to methylmercury modifies muscarinic cholinergic receptor binding characteristics in rat brain and lymphocytes: Physiologic implications and new opportunities in biologic monitoring. *Environ. Health Perspect*. **108,** 29–33.

Costa, L. G., Aschner, M., Vitalone, A., Syversen, T., and Soldin, O. P. (2004). Developmental neuropathology of environmental agents. *Annu. Rev. Pharmacol. Toxicol*. **44,** 87–110.

Costa, L.G., Giordano, G., and Guizzetti, M. (2011). Predictive models for neurotoxicity assessment. In *Predictive Toxicology in Drug Safety* (J. J. Xu and L. Urban, Eds.), pp. 135–152. Cambridge University Press, Cambridge, UK.

Crump, K. S. (1984). A new method for determining allowable daily intakes. *Fundam. Appl. Toxicol*. **4,** 854–871.

Daré, E., Fetissov, S., Hökfelt, T., Hall, H., Ogren, S. O., and Ceccatelli, S. (2003). Effects of prenatal exposure to methylmercury on dopamine-mediated locomotor activity and dopamine D2 receptor binding. *Naunyn Schmiedebergs Arch. Pharmacol*. **367,** 500–508.

de Groot, D. M., Bos-Kuijpers, M. H., Kaufmann, W. S., Lammers, J. H., O'Callaghan, J. P., Pakkenberg, B., Pelgrim, M. T., Waalkens-Berendsen, I. D., Waanders, M. M., and Gundersen, H. J. (2005). Regulatory developmental neurotoxicity testing: A model study focussing on conventional neuropathology endpoints and other perspectives. *Environ. Toxicol. Pharmacol*. **19,** 745–755.

de Groot, D. M., Hartgring, S., van de Horst, L., Moerkens, M., Otto, M., Bos-Kuijpers, M. H., Kaufmann, W. S., Lammers, J. H., O'callaghan, J. P., Waalkens-Berendsen, I. D., *et al.* (2005). 2D and 3D assessment of neuropathology in rat brain after prenatal exposure to methylazoxymethanol, a model for developmental neurotoxicty. *Reprod. Toxicol*. **20,** 417–432.

Dennis, G., Jr, Sherman, B. T., Hosack, D. A., Yang, J., Gao, W., Lane, H. C., and Lempicki, R. A. (2003). DAVID: Database for Annotation, Visualization, and Integrated Discovery. *Genome Biol*. **4,** P3.

Díez-Guerra, F. J. (2010). Neurogranin, a link between calcium/calmodulin and protein kinase C signaling in synaptic plasticity. *IUBMB Life* **62,** 597–606.

European Commission. (2006). Commission Regulation (EC) No 1881/2006 of 19 December 2006 setting maximum levels for certain contaminants in foodstuffs, issued by European Commission. *Official J. Eur. Union*, **L 364,** 5.

European Commission (DG ENV). (2010). *Review on the community strategy concerning Mercury. Final Report October 2010*. European Commission, Brussels, Belgium.

European Food Safety Authority (EFSA). (2009). Guidance of the Scientific Committee on a request from EFSA on the use of the benchmark dose approach in risk assessment. *EFSA J*. **1150,** 1–72.

Farina, M., Aschner, M., and Rocha, J. B. (2011a). Oxidative stress in MeHg-induced neurotoxicity. *Toxicol. Appl. Pharmacol*. **256,** 405–417.

Farina, M., Rocha, J. B., and Aschner, M. (2011b). Mechanisms of methylmercury-induced neurotoxicity: Evidence from experimental studies. *Life Sci*. **89,** 555–563.

Franco, J. L., Teixeira, A., Meotti, F. C., Ribas, C. M., Stringari, J., Garcia Pomblum, S. C., Moro, A. M., Bohrer, D., Bairros, A. V., Dafre, A. L., *et al.* (2006). Cerebellar thiol status and motor deficit after lactational exposure to methylmercury. *Environ. Res*. **102,** 22–28.

Giordano, G., and Costa L.G. (2012). Developmental neurotoxicity: Some old and new issues. *ISRN Toxicol.* Article ID 814795, 12.

Grandjean, P., and Herz, K. T. (2011). Methylmercury and brain development: Imprecision and underestimation of developmental neurotoxicity in humans. *Mt. Sinai J. Med*. **78,** 107–118.

Grandjean, P., and Landrigan, P. J. (2006). Developmental neurotoxicity of industrial chemicals. *Lancet* **368,** 2167–2178.

Grandjean, P., Weihe, P., White, R. F., Debes, F., Araki, S., Yokoyama, K., Murata, K., Sørensen, N., Dahl, R., and Jørgensen, P. J. (1997). Cognitive deficit in 7-year-old children with prenatal exposure to methylmercury. *Neurotoxicol. Teratol*. **19,** 417–428.

Harada, M. (1995). Minamata disease: Methylmercury poisoning in Japan caused by environmental pollution. *Crit. Rev. Toxicol*. **25,** 1–24.

Harada, Y. (1968). Congenital (or fetal) Minamata disease. In *Minamata Disease* (Study group of Minamata disease, Ed.), pp. 93–118. Kumamoto University, Japan.

Johansson, C., Castoldi, A. F., Onishchenko, N., Manzo, L., Vahter, M., and Ceccatelli, S. (2007). Neurobehavioural and molecular changes induced by methylmercury exposure during development. *Neurotox. Res*. **11,** 241–260.

Katz, B., and Miledi, R. (1968). The role of calcium in neuromuscular facilitation. *J. Physiol. (Lond.)* **195,** 481–492.

Kjellstrom, T., Kennedy, P., Wallis, S., Stewart, A., Friberg, L., and Linf, B. (1989). *Physical and Mental Development of Children With Prenatal Exposure to Mercury From Fish. Stage II Interviews and Psychological Tests at Age 6 (3642)*. National Swedish Environmental Protection Board Report, Stockholm, Sweden.

Mai, J. K., and Ashwell, K. W. S. (2004). Fetal development of the central nervous system. In *The Human Nervous System* (G. Paxinos and J. K. Mai, Eds.), 2nd ed., pp. 49–94. Elsevier, Amsterdam.

Manfroi, C. B., Schwalm, F. D., Cereser, V., Abreu, F., Oliveira, A., Bizarro, L., Rocha, J. B., Frizzo, M. E., Souza, D. O., and Farina, M. (2004). Maternal milk as methylmercury source for suckling mice: Neurotoxic effects involved with the cerebellar glutamatergic system. *Toxicol. Sci*. **81,** 172–178.

Miledi, R., and Thies, R. (1971). Tetanic and post-tetanic rise in frequency of miniature end-plate potentials in low-calcium solutions. *J. Physiol. (Lond.)* **212,** 245–257.

Organisation for Economic Co-operation and Development (OECD). (2007). *OECD Guidelines for the Testing of Chemicals/Section 4: Health Effects, Test No. 426: Developmental Neurotoxicity Study*. ISBN: 9789264067394, OECD Code: 979942601E1, Version: E-book (PNDF Format), 26. OECD, France.

Paletz, E. M., Craig-Schmidt, M. C., and Newland, M. C. (2006). Gestational exposure to methylmercury and n-3 fatty acids: Effects on high- and low-rate operant behavior in adulthood. *Neurotoxicol. Teratol*. **28,** 59–73.

Parnas, H., Dudel, J., and Parnas, I. (1982). Neurotransmitter release and its facilitation in crayfish. I. Saturation kinetics of release, and of entry and removal of calcium. *Pflugers Arch*. **393,** 1–14.

Prichard, L., Deloulme, J. C., and Storm, D. R. (1999). Interactions between neurogranin and calmodulin in vivo. *J. Biol. Chem*. **274,** 7689–7694.

Psarros, M., Heber, S., Sick, M., Thoppae, G., Harshman, K., and Sick, B. (2005). RACE: Remote Analysis Computation for gene Expression data. *Nucleic Acids Res*. **33**(Web Server issue), W638–W643.

Radonjic, M., de Haan, J. R., van Erk, M. J., van Dijk, K. W., van den Berg, S. A., de Groot, P. J., Müller, M., and van Ommen, B. (2009). Genome-wide mRNA expression analysis of hepatic adaptation to high-fat diets reveals switch from an inflammatory to steatotic transcriptional program. *PLoS ONE* **4,** e6646.

Sakamoto, M., Kakita, A., Wakabayashi, K., Takahashi, H., Nakano, A., and Akagi, H. (2002). Evaluation of changes in methylmercury accumulation in the developing rat brain and its effects: A study with consecutive and moderate dose exposure throughout gestation and lactation periods. *Brain Res*. **949,** 51–59.

Slob, W. (2002). Dose-response modeling of continuous endpoints. *Toxicol. Sci*. **66,** 298–312.

Smyth, G. K. (2004). Linear models and empirical bayes methods for assessing differential expression in microarray experiments. *Stat. Appl. Genet. Mol. Biol*. **3,** Article3.

Spyker, J. M., Sparber, S. B., and Goldberg, A. M. (1972). Subtle consequences of methylmercury exposure: Behavioral deviations in offspring of treated mothers. *Science* **177,** 621–623.

Stanford, I. M., Wheal, H. V., and Chad, J. E. (1995). Bicuculline enhances the late GABAB receptor-mediated paired-pulse inhibition observed in rat hippocampal slices. *Eur. J. Pharmacol*. **277,** 229–234.

Takeuchi, T. (1985). Human effects of methyl mercury as an environmental neurotoxicant. In *Neurotoxicology* (K. Blum and L. Manzo, Eds.), pp. 345–367. Marcel Dekker, Inc., New York, NY.

Takizawa, Y., and Kitamura, S. (2001). Estimation of the incidence of mercury exposure in the Minamata and Niigata areas using mathematical model from Iraqi poisoning. In *Understanding Minamata disease: Methylmercury Poisoning in Minamata and Niigata Japan* (Y. Takizawa and M. Osame, Eds.), pp. 27–32. Japan Public Health Association, Tokyo.

Tao, W., and Lai, E. (1992). Telencephalon-restricted expression of BF-1, a new member of the HNF-3/fork head gene family, in the developing rat brain. *Neuron* **8,** 957–966.

The Experiments on Animals Act, According to Dutch Law. (1977). Available at: http://wetten.overheid.nl/BWBR0003081.

Tonk, E. C., de Groot, D. M., Penninks, A. H., Waalkens-Berendsen, I. D., Wolterbeek, A. P., Slob, W., Piersma, A. H., and van Loveren, H. (2010). Developmental immunotoxicity of methylmercury: The relative sensitivity of developmental and immune parameters. *Toxicol. Sci*. **117,** 325–335.

U.S. Environmental Protection Agency (US EPA). (1996). Health Effects Test Guidelines: OPPTS 870.8600 Developmental neurotoxicity screen ("Public Draft"), EPA712–C–96–258, June 1996, 9 pages.

U.S. Environmental Protection Agency (US EPA). (1998). Health Effects Test Guidelines OPPTS 870.6300 Developmental Neurotoxicity Study, EPA 712–C–98–239, August 1998, 12 pages.

Weiss, B., Stern, S., Cox, C., and Balys, M. (2005). Perinatal and lifetime exposure to methylmercury in the mouse: Behavioral effects. *Neurotoxicology* **26,** 675–690.

Zucker, R. S. (1989). Short-term synaptic plasticity. *Annu. Rev. Neurosci*. **12,** 13–31.